Int. J. Electrochem. Sci., 12 **(2017)** 11137 – 11149, doi: 10.20964/2017.12.58

International Journal of
ELECTROCHEMICAL
SCIENCE
www.electrochemsci.org

Inhibition of AA 2024-T3 Corrosion in Alkaline NaCl Solution by Compound Sodium Dodecylbenzenesulfonate and Cerium Chloride

Yu Zuo, Biner Zhou and Yuming Tang[*]

Beijing Key Laboratory of Electrochemical Process and Technology for Materials,
Beijing University of Chemical Technology, Beijing 100029, China
[*]E-mail: tangym@mail.buct.edu.cn

Received: 1 July 2017 / *Accepted:* 29 September 2017 / *Published:* 12 November 2017

The synergic corrosion inhibition of AA 2024-T3 by sodium dodecylbenzenesulfonate and cerium chloride in 0.01 mol/L NaCl solution (pH 10) was studied by potentiodynamic polarization, XPS, EDS and SEM. In presence of 0.1 g/L $CeCl_3$ + 0.28 g/L SDBS inhibitors, both the general corrosion and pitting corrosion were effectively inhibited. A compound inhibition film including the oxides and hydroxides of aluminum and cerium, the organic rare earth compound $Ce(DBS)_3$ and the corrosion product $Al(DBS)_3$ were formed on the surface, which provided good corrosion protection to the AA substrate. As the immersion time was extended, the passive state remained stable while the inhibition effect for pitting corrosion decreased to some extent due to the formation of pits around the Cu-rich phases, induced by the galvanic effect between the Cu-rich phases and the aluminum substrate.

Keywords: AA 2024-T3; Inhibition; SDBS; $CeCl_3$; Pitting corrosion

1. INTRODUCTION

The 2024-T3 aluminum alloy is widely used in industrial applications due to its high specific strength and good corrosion resistance; however, in environments containing chloride ions, aluminum alloys may experience corrosion damages, such as pitting and intergranular corrosion. The application of corrosion inhibitors is one of the most practical methods for corrosion protection. Among various inhibitors, chromates have proven to be the excellent choice for aluminum alloys [1], but their use is being reduced because of their toxicity and carcinogenic nature [2]. Rare earth compounds offer possible alternatives for many of these applications [3]. It was reported [4] that rare earth salts provide good protection for aluminum alloys. Hinton's studies [5] showed that many types of rare earth

metallic ions have good inhibition effects on corrosion of aluminum alloys in neutral NaCl solutions. The rare earth salts are cathodically deposited inhibitors, which can reduce corrosion by forming rare earth oxides/hydroxides films on the surface of the alloy, reducing the rate of reaction with oxygen [6,7]. Many organic inhibitors also show good inhibition effects towards the corrosion of metals by forming protective films on the surface through physical or chemical adsorption [8]. Qafsaoui et al. [9] found that 1-pyrrolidine dithiocarbamate (PDTC) exercises very good corrosion protection on the AA 2024 alloy because it forms an adsorbed film on the Cu-rich surface and decreases the alloy reactivity. Balaskas et al. [10] and Hosseini et al. [11] studied the inhibition effect of 2-mercaptobenzothiazole (MBT) and sodium dodecylbenzenesulfonate (SDBS) on aluminum alloy and mild steel. Some authors studied the inhibitive effects of compounds of rare earth salts with organic inhibitors, in order to further increase the inhibition efficiency of the rare earth inhibitors and decrease their cost [12-14]. Forsyth et al. [15] found that cerium chloride and sodium salicylate show a synergistic inhibition effect for mild steel in a neutral NaCl solution. Kartsonakis et al. [12] found that cerium and molybdate ions together with MBT have good inhibition action on corrosion of AA 2024-T3 alloy. Catubig et al. [16] studied the inhibition effects of thioglycollate acid rare earth salts, prepared by compounding sodium thioglycollate with cerium chloride or praseodymium chloride respectively, for AA2024-T3 in NaCl solution. Liu et al. [14] reported that in NaCl solution, cerium nitrate and SDBS show very good synergistic inhibition effects for the AA5052 aluminum alloy.

So far, there have been few studies on the corrosion inhibition of aluminum alloys by rare earth salts and SDBS in basic NaCl environments. Also, studies on the effect of inhibitors on pitting corrosion, which can take place on aluminum alloys in NaCl solutions, are limited. Previously we studied the inhibition effects of $LaCl_3$ and SDBS for AA 2024 in an NaCl solution and a synergic inhibition effect was reported [17]. $CeCl_3$ has been known as an effective rare earth inhibitor for aluminum alloys for many years [18-20]. According to Mishra [21], both $CeCl_3$ and $LaCl_3$ were good inhibitors for AA 2024 in 3.5% NaCl, and $CeCl_3$ showed a better inhibition effect than $LaCl_3$. The study by Wilson and Forsyth [15] indicated that the incorporation of Ce^{3+} and the carboxylate anion may strengthen the inhibitive effect, and the salicylate cerium was formed by the reaction between $CeCl_3$ and sodium salicylate showed good inhibition for steel in NaCl solution. The compounds formed by Ce^{3+} and La^{3+} ions with cinnamic acid or cinnamates also showed good inhibition [22-24].

Based on the previous findings, it is reasonable to expect a synergistic inhibition effect of cerium salt and SDBS. The alkaline NaCl solution is a severe environment for aluminum alloys. In this paper, the inhibition effects of compound $CeCl_3$ and SDBS inhibitors on AA2024-T3 in 0.01 mol/L NaCl (pH 10) were studied, and the inhibiting mechanism was discussed.

2. EXPERIMENTAL

The studied material was a 2024-T3 aluminum alloy (AA2024-T3) with nominal chemical composition (wt.%) of Si 0.5, Fe 0.5, Cu 3.8-4.9, Mn 0.3-0.9, Mg 1.2-1.8, Cr 0.1, Zn 0.25, Ti 0.15 and Al bal.

The AA2024-T3 material was first cut into 13 mm × 13 mm × 10 mm samples. The samples were then sealed by epoxy resin and abraded sequentially with 240#, 600# and 1000# abrasive papers, rinsed in de-ionized water, degreased with acetone, and finally covered with epoxy resin leaving an area of 0.16 cm^2 exposed to the test solution.

The inhibitors used were $CeCl_3$ (reagent grade) and sodium dodecylbenzenesulfonate ($C_{12}H_{25}C_6H_4SO_3Na$, SDBS, chemical grade) produced by The Chemical Reagent Company (Beijing, China) and Fuchen Chemical Reagent Plant (Tianjin, China), respectively. 0.01 mol/L (0.58 g/L) NaCl solution was selected as the basic solution. When the $CeCl_3$ inhibitor was added, the chloride ions in $CeCl_3$ was included in the total chloride concentration count. After the addition of inhibitors, the pH of the solution was adjusted to 10 by adding NaOH and controlled with a PHS-3C pH meter (Shanghai Precise Instruments Co., China). All the other chemicals used were reagent grade. The solution was prepared with deionized water without deaeration.

The potentiodynamic polarization tests were carried out to evaluate the corrosion behavior of AA2024-T3 before and after the addition of inhibitors. Polarization curves were measured with a CS350 potentiostat (Wuhan Corrtest Instrument Co., China). The potential scanning rate was 0.3 mV/s, starting from an open circuit potential (OCP) of -0.3 V and then moving in the positive direction until pitting corrosion occurred. Before the polarization test, the working electrode was immersed in the solution for 30 min while the OCP was measured. All the experiments were carried out at room temperature in a glass cell with a saturated calomel electrode (SCE) as reference electrode, a platinum electrode as counter electrode and the aluminum alloy sample as working electrode. The corrosion current density was obtained by the Tafel extrapolation method on the cathodic branch with a CView software.

A TENSOR27 Fourier transform infrared spectrometer (FTIR) (Bruker, Germany) with measuring range 600-4000 cm^{-1} was used to study the corrosion products. The surface composition of the samples was analyzed with an ESCALAB-250 X-rays photoelectron spectrometer (XPS) (Thermo Fisher Scientific, USA). The spectra were fitted by the XPSPEAK 4.1 software. The surface morphology of the samples was observed with a LEO-1450 scanning electronic microscope (SEM) (KEVEX, USA), and the composition of the corroded surface and the corrosion products was analyzed with the Kevex SuperDry energy dispersion spectroscope (EDS).

3. RESULTS AND DISCUSSION

The polarization curves of AA 2024 in 0.01 mol/L NaCl solution (pH 10) with 0.1 g/L $CeCl_3$ plus different concentrations of SDBS inhibitors were obtained and are presented in Fig. 1. In the solution without inhibitor, the polarization curve showed an active corrosion characteristic on the anodic polarization branch. When only $CeCl_3$ was added, the polarization curve still showed the active corrosion characteristics, with a slightly increased corrosion potential, but the corrosion current density decreased obviously. This is in agreement with the results relative to the use of the $CeCl_3$ inhibitor on aluminum alloys obtained by other authors [21] and similar to the earlier study on $LaCl_3$ [17]. However, when SDBS was added in the solution, the corrosion potential (E_{corr}) decreased obviously

and a passive region appeared on the polarization curve. At higher potential, about -0.2 V_{SCE}, the current density increased suddenly, indicating the breakdown of passive film and pitting corrosion. The above results show that $CeCl_3$ did not change the corrosion mechanism but inhibited both the anodic and the cathodic reactions. SDBS also showed a mixed inhibition effect, but inhibited the anodic process more effectively and the passivation of the aluminum alloy was promoted. Hosseini [11] and Luo et al. [25] studied the corrosion inhibition of mild steel by SDBS in acidic solutions and found that SDBS inhibited both the anodic and cathodic reactions. It can also be seen that with an increase in SDBS concentration, the E_{corr} shifted negatively and the pitting potential (E_{pit}) shifted positively. In presence of 0.1 g/L $CeCl_3$ and 0.28 g/L SDBS, the polarization curve showed the widest passive range (i.e. the biggest difference between E_{corr} and E_{pit}).

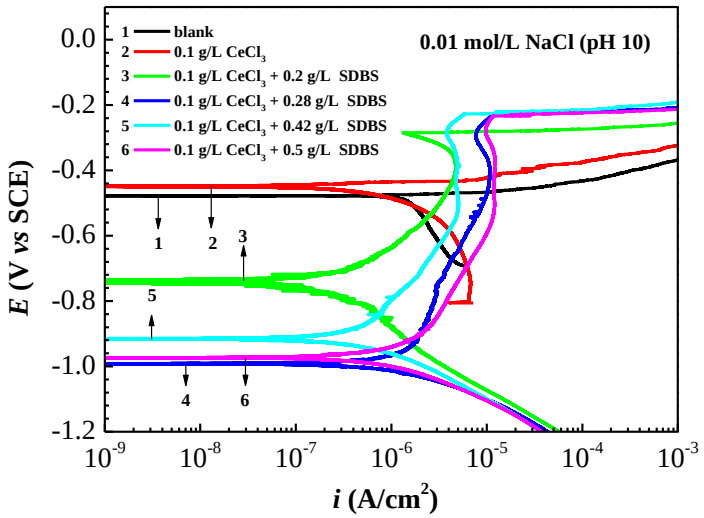

Figure 1. Potentiodynamic polarization curves for AA 2024 in 0.01 mol/L NaCl solution (pH 10) with 0.1 g/L $CeCl_3$ and different concentrations of SDBS.

Furthermore, according to above results，0.28 g/L SDBS was selected and the effect of $CeCl_3$ concentration was examined. Fig. 2 shows the polarization curves of AA 2024 in 0.01 mol/L NaCl (pH 10) solution with 0.28 g/L SDBS and different concentrations of $CeCl_3$ inhibitor. Compared with the curve obtained in the absence of inhibitor, the addition of 0.28 g/L SDBS resulted in a decreased corrosion potential E_{corr} (from -0.48 V_{SCE} to -0.61 V_{SCE}) and an apparent passive range appeared, indicating that in these conditions, SDBS acted as a mixed inhibitor [11,17,25]. When 0.05 g/L $CeCl_3$ was added, the E_{corr} further moved in the negative direction, close to -0.1 V_{SCE}. This result confirms the finding of a previous report [15] that $CeCl_3$ is predominantly cathodic, indicating that the synergistic effect of SDBS and $CeCl_3$ effectively inhibited the cathodic reaction. In the solution with 0.1 g/L $CeCl_3$ + 0.28 g/L SDBS the polarization curve shows the longest passive range and the highest pitting potential E_{pit}. With a higher $CeCl_3$ concentration, the corrosion potential increased and the passive range was shortened.

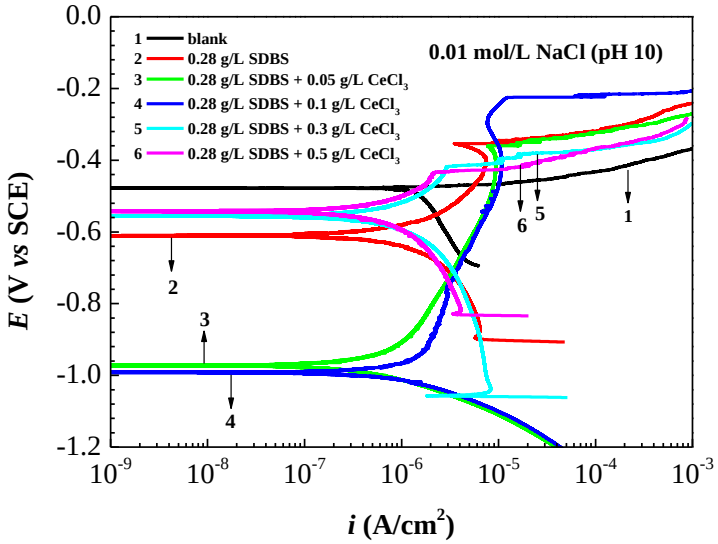

Figure 2. Potentiodynamic polarization curves for AA 2024 in 0.01 mol/L NaCl solution (pH 10) with different concentrations of $CeCl_3$ and 0.28 g/L SDBS.

The corrosion current density and the inhibition efficiency under different conditions were obtained, by Tafel extrapolation of the cathodic branches of the polarization curves, as shown in Table 1. With only 0.1 g/L $CeCl_3$ or 0.28 g/L SDBS, the inhibition efficiencies, η, were 70.54% and 90.41% respectively, but in the presence of both $CeCl_3$ and SDBS the value of η reached over 90%, showing a good synergistic inhibition effect on the general corrosion of AA 2024. It can be seen from Table 1 that $CeCl_3$ effectively increased the inhibition efficiency. When the $CeCl_3$ concentration increased from 0.1 g/L to 0.5 g/L, η increased from 91% to 96%; however, considering the influence of the inhibitors on both the general corrosion and the pitting corrosion, the best inhibition is obtained by adding 0.1 g/L $CeCl_3$ plus 0.28 g/L SDBS.

Table 1. Corrosion current density i_{corr} and inhibition efficiency η as a function of inhibitor concentrations

C_{SDBS} (g/L)	i_{corr} (μA/cm^2) (0.1 g/L $CeCl_3$)	η (%)	C_{CeCl3} (g/L)	i_{corr} (μA/cm^2) (0.28 g/L SDBS)	η (%)
0	5.6 (without $CeCl_3$)	--	0	5.6 (without SDBS)	--
0	1.65	70.54	0	0.537	90.41
0.2	0.178	96.82	0.05	0.378	93.25
0.28	0.501	91.05	0.1	0.501	91.05
0.42	0.259	95.38	0.2	0.229	95.91
0.5	0.513	90.84	0.3	0.222	96.04
			0.5	0.218	96.11

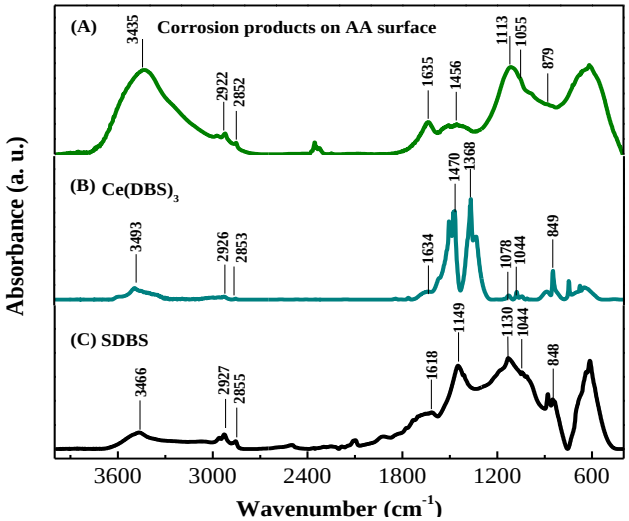

Figure 3. The measured FTIR spectra of corroded AA 2024 in 0.01 mol/L NaCl solution (pH 10) with 0.1 g/L $CeCl_3$ + 0.28 g/L SDBS, (A) corrosion products on sample surface, (B) $Ce(DBS)_3$, (C) SDBS.

After the AA sample was immersed in the test solution with 0.1 g/L $CeCl_3$ + 0.28 g/L SDBS, the corrosion product formed on the surface of the alloy was analyzed by FTIR. The results are shown in Fig. 3 and the FTIR spectra of SDBS and $Ce(DBS)_3$ are also shown for comparison. The characteristic absorption peak of the benzene ring is between 1600-1650 cm^{-1} [26] and can be seen in Figs. 3a, 3b and 3c, respectively, at 1635 cm^{-1}, 1634 cm^{-1} and 1618 cm^{-1}. The peaks at 879 cm^{-1}, 849 cm^{-1} and 848 cm^{-1} are the countpoint replace vibration peaks of the benzene ring [27]. The peaks at 2922 cm^{-1}, 2926 cm^{-1} and 2927 cm^{-1} are the antisymmetric stretching vibration peaks of -CH_2- [26,28], and the peaks at 2852 cm^{-1}, 2853 cm^{-1} and 2855 cm^{-1} are due to the symmetric stretching vibration of -CH_2- [17,19]. For SDBS and $Ce(DBS)_3$ (Fig. 3b and 3c), the peaks at 1044 cm^{-1} are attributable to the symmetrical stretching vibration peak of the S=O bond [26]. However, In Fig. 3a this peak moves to 1055 cm^{-1}. A possible reason is that the corrosion products on the surface may contain not only adsorbed DBS^- and insoluble $Ce(DBS)_3$, but also the $Al(DBS)_3$ that was formed by reaction between DBS^- and Al^{3+} [29].

Fig. 4 shows the Al2p and O1s XPS spectra of the original surface of the AA2024-T3 sample in air. It is seen that the film on the sample surface is composed mainly of Al_2O_3 and $Al(OH)_3$. The Al peak is also seen on the spectra, and since it is only present in the substrate, it shows that the passive film is very thin. Fig. 5 shows the XPS spectra of the sample surface after immersion in the test solution containing both $CeCl_3$ and SDBS. In Fig. 5a, besides Al_2O_3 and $Al(OH)_3$, there is a binding energy peak at 75.5 eV which may be attributed to $Al(DBS)_3$ [30]. This confirms the result of FTIR that $Al(DBS)_3$ may be formed by the reaction between DBS^- and dissolved Al^{+3} ions. The Fe peak cannot be discerned, suggesting the formation of an inhibition film on the surface.

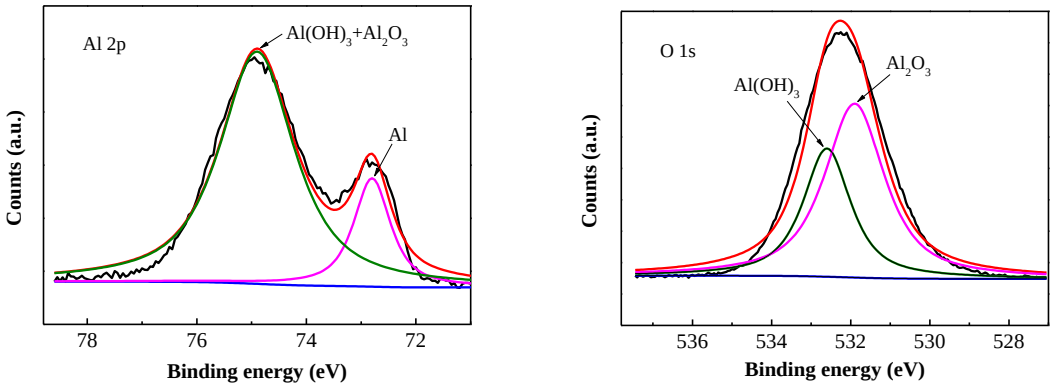

(A) (B)

Figure 4. XPS spectra for AA 2024-T3 surface in air, (A) Al 2p, (B) O 1s.

In Fig. 5b, the O1s peak at 531.6 eV may be due to the Ce-O bond and Al_2O_3 (Ce-O: O1s = 530.3 eV； Al_2O_3: O1s = 531.9 eV) [31]. The peak at 532.1 eV may contain the O-S=O [32] and Ce hydroxide (Ce-OH: O1s = 532.21 eV) groups [33]. In the C1s spectra (Fig. 5c), both the peak at 285 eV representing the linear C-C chain [34] and the peak at 284.2 eV representing the -CH= group in the benzene ring [35] are discerned. The small peak at 289.2 eV may be due to the C-S group. The above results confirm the presence of DBS on the alloy surface.

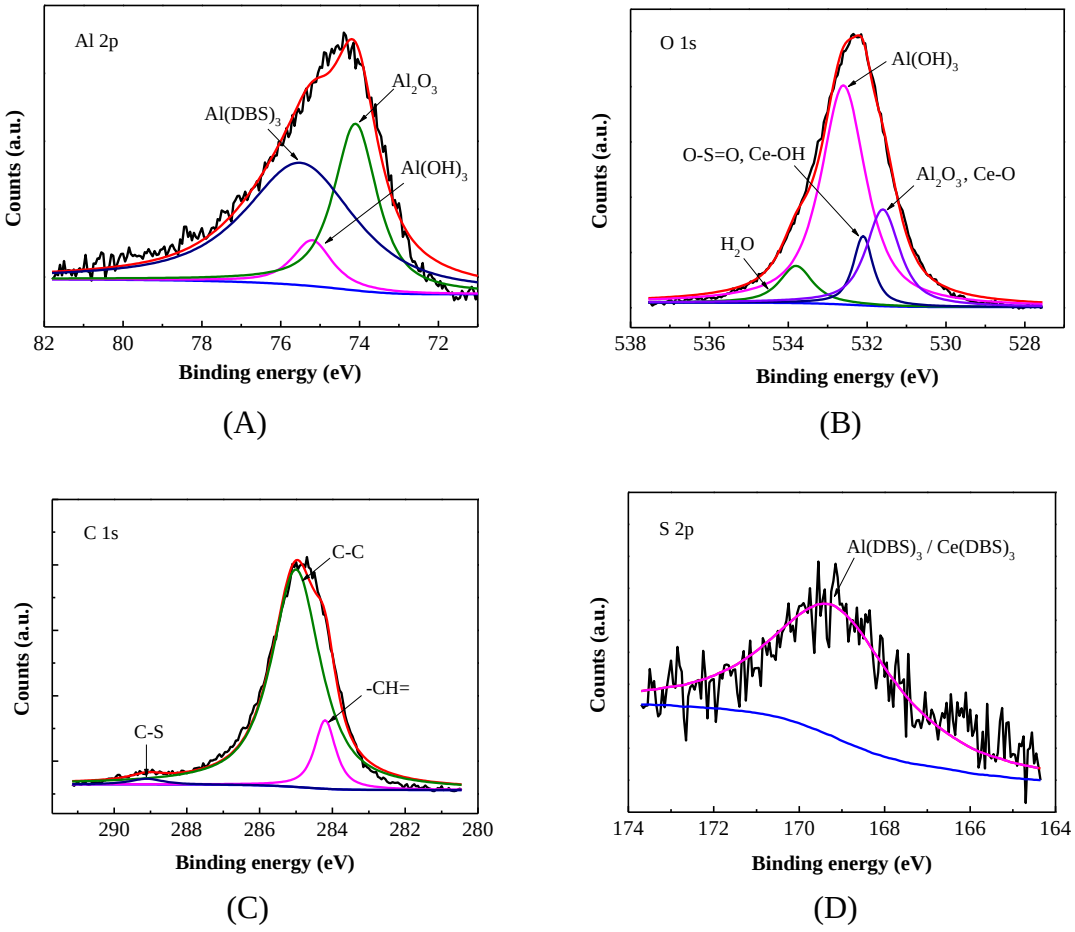

(A) (B)

(C) (D)

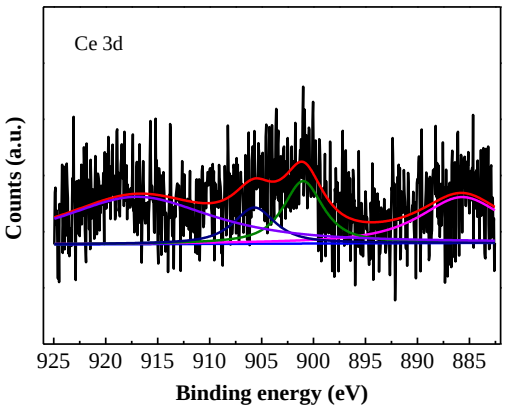

(E)

Figure 5. XPS spectra for AA 2024 surface exposure in 0.01 mol/L NaCl solution (pH 10) with 0.1 g/L $CeCl_3$ + 0.28 g/L SDBS inhibitors: (A) Al2p, (B) O1s, (C) C1s, (D) S2p, (E) Ce3d.

In the S2p spectra (Fig. 5d), the peak at 169.2 eV may be due to $Al(DBS)_3$ and Ce-DBS [30]. In the Ce3d spectra (Fig. 5e), Ce_2O_3, $Ce(OH)_3$ (885.7 eV) [35] and CeO_2 (917eV) [36] can be distinguished. In addition, double peaks at 901 and 905.7 eV are seen, which are very close to the values obtained when Ce^{3+} is bound to sulfuric acid anions [37], probably deriving from $Ce(DBS)_3$.

Fig. 6 shows the Ce and S spectra of the AA samples after immersion in the 0.01 mol/L NaCl solution (pH 10) with 0.1 g/L $CeCl_3$ + 0.28 g/L SDBS for different times. The $Ce(DBS)_3$ spectra is also shown in the figures for comparison. The Ce3d spectra show that after immersion $Ce(DBS)_3$ was formed on the surface and that its amount increased with time. The peak at 917 eV after 24 h immersion may be attributed to CeO_2. In Fig. 6b (S2p spectra) the peak at 169.2 eV is due to S in $Ce(DBS)_3$, which also confirms the formation of $Ce(DBS)_3$ on the sample surface.

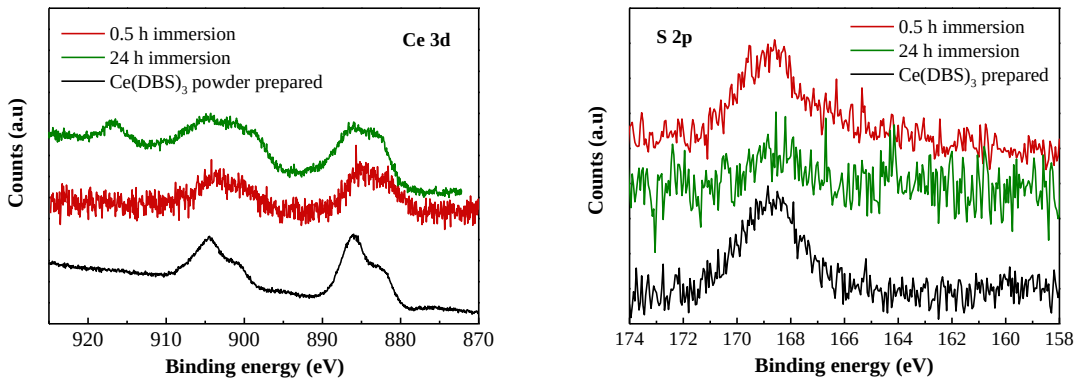

(A) (B)

Figure 6. XPS spectra for AA 2024 surface after immersion in 0.01 mol/L NaCl solution (pH 10) with 0.1 g/L $CeCl_3$ + 0.28 g/L SDBS inhibitors for different times: (A) Ce3d, (B) S2p.

Previous works have shown that the deposition of the oxides and hydroxides of cerium on aluminum alloys would protect the alloy from corrosion [38]. The above FTIR and XPS results show

that by addition of the inhibitors, beside the oxides and hydroxides of aluminum, the hydroxides and oxides of cerium, the organic rare earth compound $Ce(DBS)_3$ and the corrosion product $Al(DBS)_3$ are formed on the surface, which together provide inhibition to the AA substrate.

To further understand the effects of the inhibitors on the surface with immersion time, the open circuit potential (OCP) of a steel sample immersed in the 0.01 mol/L NaCl solution with 0.1 g/L $CeCl_3$ + 0.28 g/L SDBS was recorded with time. Fig. 7a shows that in the initial stage the OCP moved in the positive direction, indicating the adsorption and inhibition action of inhibitors on the surface. After about 5 h, the OCP reached a stable value of around -0.5 V_{SCE}, which shows that the prefilming time of $CeCl_3$ + SDBS system is shorter than that of $LaCl_3$ + SDBS system, which was about 6 h [17]. Fig. 7b shows the polarization curves of samples after immersion in the solutions for different times. With increased immersion time, the corrosion potential moved in the positive direction, and the corrosion current density values remained about the same, but the pitting potential decreased to some extent. This means that the inhibition efficiency of the $CeCl_3$ and SDBS towards pitting corrosion decreased with immersion time. Nonetheless, the polarization curves still maintained the passivation characteristics and the corrosion current density decreases noticeably, this is in contrast with the behavior observed in the absence of inhibitors, when the polarization curve portrays the typical behavior of active dissolution. It is also seen from Fig. 7b that, with a continuous immersion longer than 24 h, the corrosion potential again moved in the negative direction and the passive region on the polarization curves became broader. Usually the inhibition efficiency of inhibitors increased with prefilming time. The present results show that the compound inhibitors reached the stable inhibition in about 5 h; however, with increased time, the pitting potential decreased in some measure, which suggests that some of the factors facilitating pitting corrosion may still have been present.

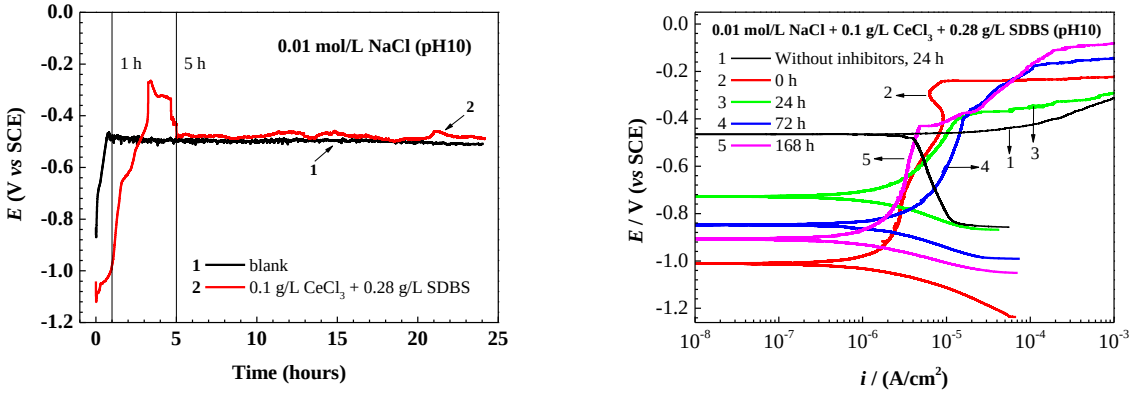

(A) (B)

Figure 7. (A) Variations of OCP of AA2024 with immersion time in 0.01 mol/L NaCl solution (pH 10) with 0.1 g/L $CeCl_3$ + 0.28 g/L SDBS, (B) Polarization curves of AA2024 after different times of immersion in 0.01 mol/L NaCl solution with or without inhibitors.

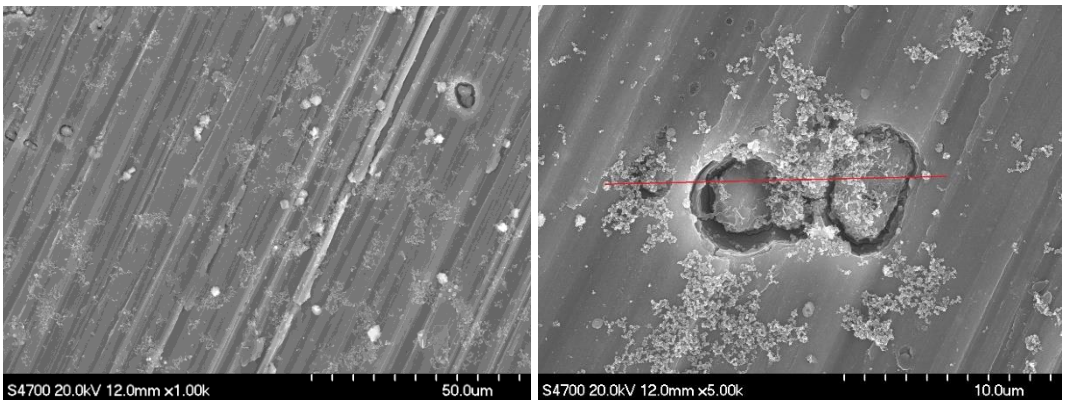

(A) (B)

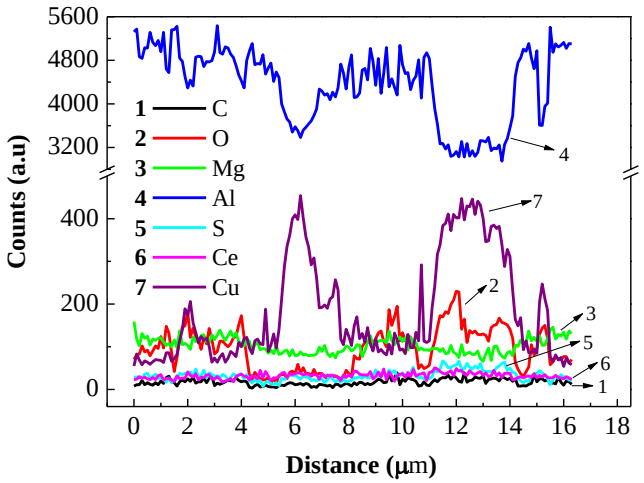

(C)

Figure 8. SEM and EDS results for AA sample after 24 h immersion in 0.01 mol/L NaCl solution (pH 10) with 0.1 g/L $CeCl_3$ + 0.28 g/L SDBS, (A, B) Surface morphology, (C) Line scan for (B).

The sample surface was examined with SEM after immersion test. Fig. 8a shows the surface image of the AA sample after immersion in the 0.01 mol/L NaCl solution with 0.1 g/L $CeCl_3$ + 0.28 g/L SDBS for 24 h. Some pits are visible on the surface. Figs. 8b and 8c show the distributions of the elements near the inclusions by EDS line scan. It is seen that the inclusions are formed by a Cu-rich phase and that dissolution occurred preferentially at the boundaries between the Cu-rich phase and the Al substrate. Similar phenomena have been reported for AA 2024 [39] and AA 2014 [21] alloys. The S phase (Al_2CuMg) is the main strengthening phase in AA2024-T3. In the Cu-rich phase Al and Mg are not detectable (Fig. 8c), which may be due to dissolution of the two elements during the corrosion process. Therefore, it could be deduced that the pits were induced by the galvanic effect between the Cu-rich phase, probably the S phase, and the substrate, which might influence the inhibition effect on pitting corrosion.

Catubig et al. [16] reported a similar phenomenon for AA2024-T3 in a neutral 0.1 M NaCl solution, in which corrosion was observed to preferentially occur around the S phase after 24 h immersion. The authors also reported the inhibition effect of the thiol-containing mercaptoacetate coupled with cerium or praseodymium. A layer of oxides and hydroxides of Al and Ce formed on the

passivated aluminum surface, while over the Cu-rich S phase some organic cerium compounds may have been deposited, considerably inhibiting corrosion. The present results also show that by forming a complicated inhibition film, including hydroxides and oxides of cerium, organic rare earth compound $Ce(DBS)_3$ and the corrosion product $Al(DBS)_3$, the compound $CeCl_3$ and SDBS inhibitors act on AA 2024 in the environment studied here so to inhibit the general corrosion and reducing, to some extent, pitting corrosion.. However, because the pH 10 solution is a relatively severe environment for aluminum alloys and the galvanic effect between the Cu rich phase and the aluminum alloy substrate might be stronger than the one observed in neutral solutions, pitting corrosion cannot be totally inhibited by the inhibitor film. With increased immersion time, the galvanic effect between the Cu rich phase and the substrate may strengthen, reducing the pitting potential. A further increase in the immersion time, on the other hand, weakens the dissolution of the substrate and induces a partial recovery of the inhibition performance of the $CeCl_3$-SDBS system. A previous study [17] showed that for AA2024 in an NaCl solution with compound $LaCl_3$ + SDBS inhibitors, the pitting potential decreased obviously after immersion and there was only a very narrow passive region left after 24 h immersion. The present results show that for the compound $CeCl_3$ + SDBS system, even after 168 h immersion (Fig. 7b) passivation was still significant and the passive region was about 600 mV wide. Therefore, compared with the $LaCl_3$ + SDBS system [17], the $CeCl_3$ + SDBS system is more effective in the inhibition of pitting corrosion of AA2024 in alkaline NaCl solutions. Mishra et al [21] studied the corrosion inhibition of AA 2014 by $LaCl_3$ and $CeCl_3$ in 3.5% NaCl solution, and the results also showed that $CeCl_3$ was a better corrosion inhibitor compared to $LaCl_3$. Davo' and Damborenea [31] reported that for AA 8090 in a 3.56% NaCl solution, $CeCl_3$ inhibited intergranular corrosion more effectively than $LaCl_3$. Both Ce and La belong to the lanthanide series and show similar characteristics. The main difference is that the outer electronic structure of La is $4f^0 5d^1 6s^2$, and that of Ce is $4f^1 5d^1 6s^2$. Therefore, the stable oxide of La is trivalent while Ce may form both trivalent and tetravalent oxides. As the result, for the inhibition system of $LaCl_3$ + SDBS, the products of La included mainly $La(OH)_3$ and $La(DBS)_3$ [17], while for the present inhibition system of $CeCl_3$ + SDBS, possible products of Ce include Ce_2O_3, $Ce(OH)_3$, $Ce(DBS)_3$ and CeO_2. Hence the inhibition films with $CeCl_3$ + SDBS addition are more stable and compact, providing better protection from corrosion to the aluminum alloy.

4. CONCLUSIONS

(1) In 0.01 mol/L NaCl solution (pH 10), $CeCl_3$ and SDBS showed a synergic inhibition effect for the AA2024-T3 aluminum alloy. $CeCl_3$ inhibited both the anodic and the cathodic reactions, while SDBS inhibited the cathodic process effectively and promoted passivation of the aluminum alloy. With 0.1 g/L $CeCl_3$ + 0.28 g/L SDBS inhibitors, both the general corrosion and pitting corrosion were effectively inhibited.

(2) Besides the oxides and hydroxides of aluminum, the oxides and hydroxides of cerium, the organic rare earth compound $Ce(DBS)_3$ and the corrosion product $Al(DBS)_3$ were formed on the surface. The compounded inhibition films provided inhibition to the AA substrate.

(3) As the immersion time extended, the passive state remained stable while the inhibition

effect for pitting corrosion decreased to some extent, due to the formation of pits around the Cu-rich phases, induced by the galvanic effect between the Cu-rich phases and the aluminum substrate.

ACKNOWLEDGEMENT
The authors would like to thank the National Natural Science foundation of China (Contract 51210001) for support to this work.

References

1. M.W. Kendig and R.G. Buchheit, *Corros*., 59 (2003) 379.
2. M. Kendig, S. Jeanjaquet, R. Addison and J. Waldrop, *Surf. Coat. Technol*., 140 (2001) 58.
3. G.N. Mu, X.H. Li, Q. Qu and J. Zhou, *Acta Chim. Sinica*, 62 (2004) 2386.
4. D. Ho, N. Brack, J. Scully, T. Markley, M. Forsyth and B. Hinton, *J. Electrochem. Soc*., 153 (2006) B392.
5. B.R.W. Hinton, *J. Alloy. Compd*., 180 (1992) 15.
6. A. Markley, M. Forsyth and A.E. Hughes, *Electrochim. Acta*, 52 (2007) 4024.
7. I. Milošev and P. Rodič, *Corrosion*, 72 (2016) 1021.
8. H. Cang, W.Y. Shi, J.L. Shao and Q. Xu, *Jiangsu Agric. Sci*., 40 (2012) 339.
9. W. Qafsaoui, M.W. Kendig, H. Perrot and H. Takenouti, *Corros. Sci*., 92 (2015) 245.
10. A.C. Balaskas, M. Curioni and G.E. Thompson, *Surf. Interface Anal*., 47 (2015) 1029.
11. M. Hosseini, S.F.L. Mertens and M.R. Arshadi, *Corros. Sci*., 45 (2003) 1473.
12. C.N.B. Dickason, G.B. Deacon, C.M. Forsyth, S. Hanf, O.B. Heilmann, B.R.W. Hinton, P.C. Junk, A.E. Somers, Y.Q. Tan and D.R. Turner, *Aust. J. Chem*., 70 (2017) 478.
13. I.A. Kartsonakis, E.P. Koumoulos and C.A. Charitidis, *Manuf. Rev.*, 4 (2017) 2.
14. J. Liu, D. Wang, L. Gao and D. Zhang, *Appl. Surf. Sci*., 389 (2016) 369.
15. M. Forsyth, C.M. Forsyth, K. Wilson, T. Behrsing and G.B. Deacon, *Corros. Sci*., 44 (2002) 2651.
16. R. Catubig, A.E. Hughes, I.S. Cole, B.R.W. Hinton and M. Forsyth, *Corros. Sci*., 81 (2014) 45.
17. B. Zhou, Y. Wang and Y. Zuo, *Appl. Surf. Sci*., 357 (2015) 735.
18. B.R.W. Hinton, D.R. Arnott and N.E. Ryan, *Mater. Forum*, 9 (1986) 162.
19. F. Mansfeld, S. Lin, S. Kim and H. Shih, *Electrochim. Acta*, 34 (1989) 1123.
20. F. Mansfeld and Y. Wang, *Mater. Sci. Eng*., A 198 (1995) 51.
21. A. K. Mishra and R. Balasubramaniam, *Corros. Sci*., 49 (2007) 1027.
22. F. Blin, S.G. Leary, K. Wilson, G.B. Deacon, P.C. Junk and M. Forsyth, *J. Appl. Electrochem*., 34 (2004) 591.
23. T. Hu, H. Shi, T. Wei, F. Liu, S. Fan and E. Han, *Corros. Sci*., 95 (2015) 152.
24. T.Hu, H. Shi, S. Fan, F. Liu E. Han, *Prog. Org. Coat*., 105 (2017) 123.
25. H. Luo, Y.C. Guan and K.N. Han, *Corros*., 54 (1998) 619.
26. Y.F. Chen, R.Y. Chen, X. Zheng, X. Zheng, X. Chen and Z. Chen, *Tech. Equip. Environ. Pollut. Control*, 5 (2004) 42.
27. M. Wang, *Chin. J. Spectrosc. Lab*., 29 (2012) 138.
28. L.V. Daimay, B.C. Norman and G.F. William, The handbook of infrared and raman characteristic frequencies of organic molecules. New York: Academic Press, 1991
29. H.M. Li, Z.G. Shen, J. Wang, F.M Zhu and S.A. Lin, *J. Polym.*, 5 (2001) 599.
30. V.W.L. Lim, S. Li, E.T. Kang, K.G. Neoh and K.L. Tan, *Synth. Met*., 106 (1999) 1.
31. B. Davó and J.J. de Damborene, *Electrochim. Acta*, 49 (2004) 4957.
32. X.L. Tan, M. Fang, C.L. Chen, S.M. Yu and X.K. Wang, *Carbon*, 46 (2008) 1741.
33. S. Niroumandrad, M. Rostani and B. Ramezanzadeh, *Appl. Surf. Sci*., 357 (2015) 2121.

34. C.S. Zhang, M.F. Yan and Z. Sun, *Appl. Surf. Sci*., 287 (2013) 381.
35. H.W Shi, E.H. Han and F. C. Liu, *Corros. Sci*., 53 (2011) 2374.
36. Y. Uwamino and T. Ishizuka, *J. Electron Spectrosc. Relat. Phenom*., 34 (1984) 67.
37. H.W. Shi, E.H. Han, S.V. Lamaka, M.L. Zheludkevich, F.C Liu and M.G.S. Ferreira, *Prog. Org. Coat*., 77 (2014) 765.
38. A.E. Hughes, R.J. Taylor, B.R.W. Hinton and L. Wilson, *Surf. Interface Anal*., 23 (1995) 540.
39. V. Guillaumin, G. Mankowski, *Corros. Sci*. 41 (1998) 421.